High-frequency InGaAs tri-gate MOSFETs with fmax of 400 GHz

Zota, C. B.; Lindelöw, F.; Wernersson, L. E.; Lind, E.

Published in:
Electronics Letters

DOI:
10.1049/el.2016.3108

2016

Document Version:
Peer reviewed version (aka post-print)

High-Frequency InGaAs Tri-gate MOSFETs with f_{max} of 400 GHz

C. B. Zota, F. Lindelöw, L.-E. Wernersson and E. Lind

We report on extremely scaled down tri-gate RF MOSFETs utilizing lateral nanowires as the channel, with gate length and nanowire width both of 20 nm. These devices exhibit simultaneous extrapolated f_t and f_{max} of 275 and 400 GHz at V_{DS} = 0.5 V, which is the largest combined f_t and f_{max}, as well as the largest f_{max} reported for all III-V MOSFET.

Introduction: Tri-gate (or non-planar) MOSFETs for RF-applications are motivated by that the use of a high-k oxide, rather than a semiconductor barrier (as in HEMTs) allows for higher gate capacitance in the MOSFET [1-2]. Furthermore, the tri-gate architecture improves short-channel effects, allowing for shorter gate length, L_G, without degradation of performance due to short-channel effects. Both these points enable higher ideal transconductance, g_m, in MOSFETs compared to HEMTs, assuming similar electron mobility. In fact, state-of-the-art III-V MOSFET devices exhibit g_m larger than that of record HEMTs, although they presently do not allow RF-compatible device designs [3-5].

In this work, we present RF-compatible tri-gate $In_{0.85}Ga_{0.15}As$ MOSFETs utilizing lateral nanowires (NWs) as the channel. Compared to our previous work, we have here further scaled down device dimensions, L_G and nanowire width, W_{NW} [6]. This enables higher g_m at V_{DS} = 0.5 V, which significantly improves f_t/f_{max} from 220/305 GHz to 275/400 GHz. The combined f_t and f_{max}, as well as the f_{max} of these devices represent the highest reported values for all III-V MOSFETs.

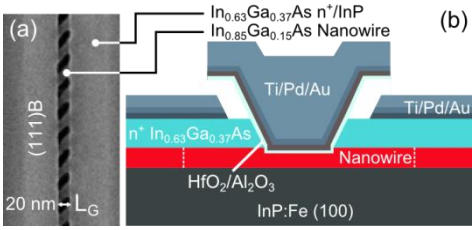

Fig. 1 *Device fabrication and device materials and design*
a SEM image of the device after contact regrowth, L_G is defined as the distance between n^+ contacts. (111)B denotes the crystal facet of the contact layer.
b Schematic figure of the fabricated device.

Fabrication: The device fabrication process is similar to what has been described elsewhere [7]. The device channel consists of 200 lateral $In_{0.85}Ga_{0.15}As$ nanowires, formed by selective area MOCVD growth on (100) InP:Fe (S.I.) substrate, split over two gate fingers. The nanowire width is 20 nm, and the height is 11 nm. The S/D highly doped regions are formed by a second MOCVD growth step of 40 nm n^+ $In_{0.63}Ga_{0.37}As$/100 nm InP with in-situ Sn-doping ($N_D = 5\times10^{19}$ cm^{-3}) in the doped layer (Fig. 1a). Subsequently, 1 nm/5 nm Al_2O_3/HfO_2 is deposited by ALD and Ti/Pd/Au by thermal evaporation, forming the gate stack. The regrown 100 nm InP is selectively etched by an HCl solution leaving a T-gate. S/D and pad metallization of Ti/Pd/Au completes the process (Fig. 1b).

Results: Fig. 2a shows transfer characteristics of a device with L_G = 20 nm measured at DC with a Keithley 4200 semiconductor characterization system. All data is normalized to the total gated periphery of the NWs (7 µm). At V_{DS} = 0.5 V, peak g_m is 2.1 mS/µm. Fig. 2b shows the scaling behaviour of peak g_m and on-resistance R_{on} versus L_G. R_{on} reaches 220 Ωµm at L_G = 20 nm. The total access resistance is estimated to 130 Ωµm from transmission line measurements.

RF-measurements where performed at 40 MHz to 67 GHz with an Agilent E8361A vector network analyser. On-chip pad de-embedding as well as off-chip two-port load-reflect-reflect-match calibration was performed. The total pad capacitances were approximately 20 fF.

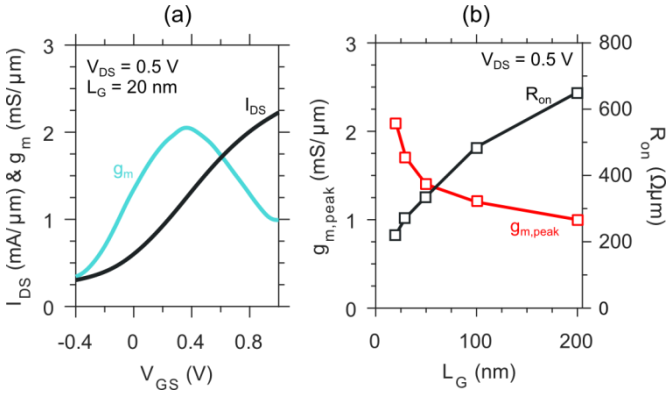

Fig. 2 *Device characteristics at DC.*
a Transfer characteristics of a L_G = 20 nm device.
b Scaling behaviour of peak g_m and R_{on} versus L_G.

A small-signal model was determined from the measured S-parameters, with a good fit to the measurement data [8]. Fig. 3 shows measured and modelled (dashed traces) unilateral power gain $|U|$, current gain $|h_{21}|^2$ and maximum available/stable gain (|MAG| and |MSG|) for a device with L_G = 20 nm. Extrapolated cut-off frequency f_t is 275 GHz and maximum oscillation frequency f_{max} is 400 GHz.

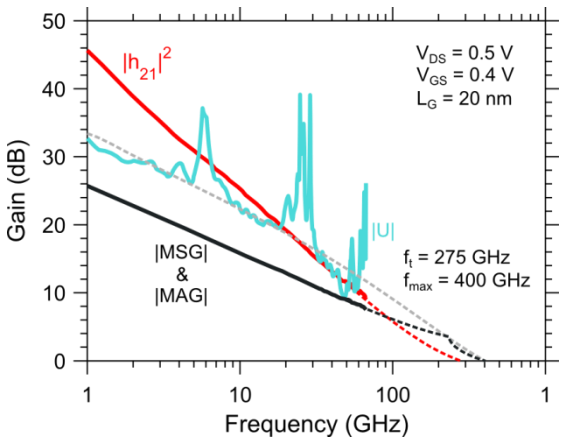

Fig. 3 *Measured and modelled (dashed traces) gain of an L_G = 20 nm device at V_{DS} = 0.5 V.*

The small-signal model, which is similar to that in [6], includes both the effect of border traps in the oxide, and impact ionization. Border traps are modelled using the distributed border trap model in [9]. Border traps introduce a frequency-dependency to g_m and g_d, as well as a frequency-dependent oxide loss, and explain the -10 dB slope of $|U|$ versus f [10]. Fig. 4a shows $g_{m,peak}$ for an L_G = 20 nm device extracted from the small-signal model at DC and 67 GHz (RF). $g_{m,peak}$ increases by approximately 13% in the latter case, to a maximum of 2.9 mS/µm at V_{DS} = 1.25 V, which is attributable to that trap responses are partially disabled at high frequency.

The effective gate resistance is ~5 Ω, and the source and drain resistances are ~2 Ω. The gate-to-source and gate-to-drain capacitances, C_{GS} and C_{GD}, are shown in Fig. 4b. At V_{DS} = 0.5 V, the total gate capacitance C_{GS} + C_{GD} is 15 fF at peak g_m. This includes both the parasitic capacitance from the source and drain gate overlaps, and the intrinsic gate capacitance. The latter is estimated as $C_{gg,int} = (2/3)WLC_{ox}/(C_q + C_{ox})$, with the quantum capacitance $C_q = q^2m^*/\pi\hbar^2$, which is ~2 fF with $m^* = 0.04m_0$. Thus, RF-performance is primarily limited by the parasitic overlap capacitance, which can be lowered by implementation of source and drain spacers.

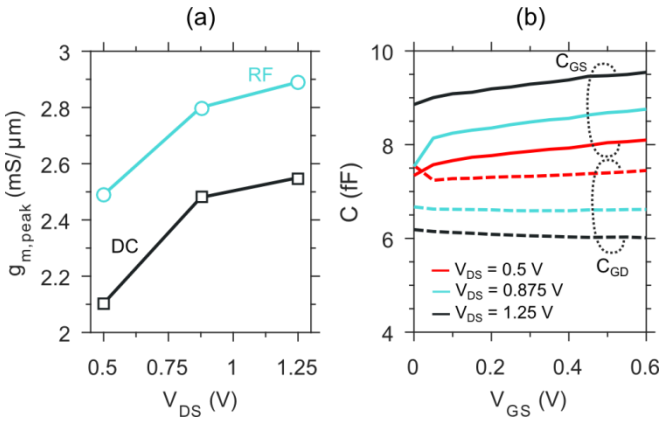

Fig. 4 *Peak g_m and capacitances*
a Peak g_m measured at both 40 MHz (DC) and 67 GHz (RF), for an L_G = 20 nm device.
b Gate-to-source, C_{GS}, and gate-to-drain, C_{GD}, capacitances measured at different V_{DS}.

Fig. 5 shows a benchmark of f_t, f_{max} and the geometric mean $\sqrt{f_t \times f_{max}}$ (dashed traces) for state-of-the-art III-V MOSFETs [11-18]. The geometric mean is 330 GHz for these devices, which is the highest reported value for a III-V MOSFET. Squares show planar devices, and triangles show non-planar devices.

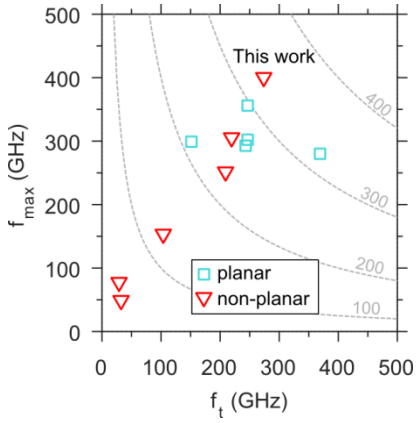

Fig. 5 *Benchmark of RF-performance for III-V MOSFETs*
Squares show planar devices, triangles show non-planar devices. V_{DS} and L_G varies between devices, but is 0.5 V and 20 nm, respectively, for this work. Dashed traces show the geometric mean.

Conclusion: We have demonstrated L_G = 20 nm $In_{0.85}Ga_{0.15}As$ tri-gate MOSFETs with record high-frequency performance, f_t = 275 GHz and f_{max} = 400 GHz at V_{DS} = 0.5 V.

Acknowledgements: This work was supported in part by the Swedish Research Council, in part by the Knut and Alice Wallenberg Foundation, in part by the Swedish Foundation for Strategic Research and in part by the European Union H2020 program INSIGHT (Grant Agreement No. 688784).

C. B. Zota, F. Lindelöw, L.-E. Wernersson and E. Lind (*Department of Electrical and Information Technology, Lund University, Box 118 S-221 00, Lund, Sweden)*

E-mail: cezar.zota@eit.lth.se

References

[1] H. Riel, L.-E. Wernersson, M. Hong, and J. a. del Alamo, "III–V compound semiconductor transistors—from planar to nanowire structures," *MRS Bull.*, 2014, **39**(08), pp. 668–677, DOI: 10.1557/mrs.2014.137
[2] D.-H. Kim, B. Brar, and J. A. del Alamo, "f_T = 688 GHz and f_{max} = 800 GHz in L_g = 40 nm $In_{0.7}Ga_{0.3}As$ MHEMTs with g_{m_max} > 2.7 mS/μm," Proc. IEEE Int. Electron Device Meeting (IEDM), Dec. 2011, pp. 13.6.1–13.6.4, 2011, DOI: 10.1109/IEDM.2011.6131548
[3] C. B. Zota, L. E. Wernersson, and E. Lind, "Single suspended InGaAs nanowire MOSFETs," Proc. IEEE Int. Electron Device Meeting (IEDM), Washington, D.C., Dec. 2015, pp. 31.4.1–31.4.4, DOI: 10.1109/IEDM.2015.7409808
[4] J. Lin, X. Cai, Y. Wu, D. A. Antoniadis, and J. A. Del Alamo, "Record maximum transconductance of 3.45 mS/μm for III-V FETs," IEEE Electron Device Lett., 2016, **37**(4), pp. 381–384, DOI: 10.1109/LED.2016.2529653
[5] S. Lee, V. Chobpattana, C.-Y. Huang, B. J. Thibeault, W. Mitchell, S. Stemmer, A. C. Gossard, and M. J. W. Rodwell, "Record I_{on} (0.50 mA/μm at V_{DD} = 0.5 V and I_{off} = 100 nA/μm) 25 nm-gate-length ZrO_2/InAs/InAlAs MOSFETs," 2014 Symp. VLSI Technol. Dig. Tech. Pap., June 2014, pp. 1–2, DOI: 10.1109/VLSIT.2014.6894363
[6] C. B. Zota, G. Roll, L.-E. Wernersson, and E. Lind, "Radio-Frequency Characterization of Selectively Regrown InGaAs Lateral Nanowire MOSFETs," *IEEE Trans. Electron Devices*, 2014, **61**(12), pp. 4078–4083, DOI: 10.1109/TED.2014.2363732
[7] C. B. Zota, D. Lindgren, L. E. Wernersson, and E. Lind, "Quantized Conduction and High Mobility in Selectively Grown InxGa1-xAs Nanowires," ACS Nano, 2015, **9**(10), pp. 9892–9897, DOI: 10.1021/acsnano.5b03318
[8] I. Kwon, M. Je, K. Lee, and H. Shin, "A simple and analytical parameter-extraction method of a microwave MOSFET," *IEEE Trans. Microw. Theory Tech.*, 2002, **50**(6), pp. 1503–1509, DOI: 10.1109/TMTT.2002.1006411
[9] Y. Yuan, L. Wang, B. Yu, B. Shin, J. Ahn, P. C. Mcintyre, P. M. Asbeck, M. J. W. Rodwell, and Y. Taur, "*A Distributed Model for Border Traps in Al_2O_3-InGaAs MOS devices*," 2011, **32**(4), pp. 485–487, DOI: 10.1109/LED.2011.2105241
[10] S. Johansson, M. Berg, K.-M. Persson, and E. Lind, "A High-Frequency Transconductance Method for Characterization of High-k Border Traps in III-V MOSFETs," *IEEE Trans. Electron Devices*, 2013, **60**(2), pp. 776–781, DOI: 10.1109/TED.2012.2231867
[11] J. Mo, E. Lind, and L.-E. Wernersson, "Asymmetric InGaAs/InP MOSFETs With Source/Drain Engineering," *IEEE Electron Device Lett.*, 2014, **35**(5), pp. 515–517, DOI: 10.1109/LED.2014.2308925
[12] T. Kim, R. J. W. Hill, C. D. Young, D. Veksler, L. Morassi, S. Oktybrshky, J. Oh, C. Y. Kang, D. Kim, J. A. Alamo, C. Hobbs, P. D. Kirsch, and R. Jammy, "InAs Quantum-Well MOSFET (L_g = 100 nm) with Record High g_m , f_T and f_{max}," 2012 Symp. VLSI Technol. Dig. Tech. Pap., June 2012, pp. 179–180, DOI: 10.1109/VLSIT.2012.6242520
[13] K. D. Chabak, X. Miao, C. Zhang, S. Member, D. E. Walker, P. K. Mohseni, X. Li, and S. Member, "RF Performance of Planar III – V Nanowire-Array Transistors Grown by Vapor – Liquid – Solid Epitaxy," 2015, **36**(5), pp. 445–447, DOI: 10.1109/LED.2015.2416978
[14] S. Johansson, E. Memisevic, L.-E. Wernersson, and E. Lind, "High-Frequency Gate-All-Around Vertical InAs Nanowire MOSFETs on Si Substrates," *IEEE Electron Device Lett.*, 2014, **35**(5), pp. 518–520, DOI: 10.1109/LED.2014.2310119
[15] D.-H. Kim, J. A. del Alamo, D. A. Antoniadis, J. Li, J.-M. Kuo, P. Pinsukanjana, Y.-C. Kao, P. Chen, A. Papavasiliou, C. King, E. Regan, M. Urteaga, B. Brar, and T.-W. Kim, "L_g = 60 nm recessed $In_{0.7}Ga_{0.3}As$ metal-oxide-semiconductor field-effect transistors with Al_2O_3 insulator," *Appl. Phys. Lett.*, 2012, **101**(22), p. 223507, DOI: 10.1063/1.4769230
[16] M. Berg, O. Kilpi, K. Persson, J. Svensson, M. Hellenbrand, E. Lind, and L.-E. Wernersson, "Electrical Characterization and Modeling of Gate-Last Vertical InAs Nanowire MOSFETs on Si," 2016, **37**(8), pp. 966–969, DOI: 10.1109/LED.2016.2581918
[17] K. Dae-Hyun, K. Tae-Woo, R. J. W. Hill, C. D. Young, K. Chang Yong, C. Hobbs, P. Kirsch, J. A. del Alamo, and R. Jammy, "High-Speed E-Mode InAs QW MOSFETs With Al2O3 Insulator for Future RF Applications," *Electron Device Lett. IEEE*, 2013, **34**(2), pp. 196–198, DOI: 10.1109/LED.2012.2229107
[18] M. Egard, L. Ohlsson, M. Ärlelid, K. Persson, B. M. Borg, F. Lenrick, R. Wallenberg, E. Lind, and L. Wernersson, "High-Frequency Performance of Self-Aligned," *IEEE Electron Device Lett.*, 2012, **33**(3), pp. 369–371, 10.1109/LED.2011.2181323